Cellular/Molecular

Cross-Species Conservation of Open-Channel Block by Na Channel β4 Peptides Reveals Structural Features Required for Resurgent Na Current

Amanda H. Lewis[1] **and Indira M. Raman**[2]

[1]Interdepartmental Biological Sciences Program and [2]Department of Neurobiology and Physiology, Northwestern University, Evanston, Illinois 60208

Voltage-gated Na channels in many neurons, including several in the cerebellum and brainstem, are specialized to allow rapid firing of action potentials. Repetitive firing is facilitated by resurgent Na current, which flows upon repolarization as Na channels recover through open states from block by an endogenous protein. The best candidate blocking protein to date is $Na_V\beta4$. The sequence of this protein diverges among species, however, while high-frequency firing is maintained, raising the question of whether the proposed blocking action of the $Na_V\beta4$ cytoplasmic tail has been conserved. Here, we find that, despite differences in the $Na_V\beta4$ sequence, Purkinje cells isolated from embryonic chick have resurgent currents with kinetics and amplitudes indistinguishable from those in mouse Purkinje cells. Furthermore, synthetic peptides derived from the divergent $Na_V\beta4$ cytoplasmic tails from five species have the capacity to induce resurgent current in mouse hippocampal neurons, which lack a functional endogenous blocking protein. These data further support a blocking role for $Na_V\beta4$ and also indicate the relative importance of different residues in inducing open-channel block. To investigate the contribution of the few highly conserved residues to open-channel block, we synthesized several mutant peptides in which the identities and relative orientations of a phenylalanine and two lysines were disrupted. These mutant peptides produced currents with vastly different kinetics than did the species-derived peptides, suggesting that these residues are required for an open-channel block that approximates physiological resurgent Na current. Thus, if other blocking proteins exist, they may share these structural elements with the $Na_V\beta4$ cytoplasmic tail.

Introduction

Resurgent Na current results from open-channel block and unblock of voltage-gated Na channels by an endogenous blocking protein that associates with pore-forming α subunits (Raman and Bean, 1997, 2001; Grieco et al., 2002). The blocking protein binds open channels at positive voltages and is expelled upon repolarization by inwardly permeating Na ions (Aman and Raman, 2010). Unlike inactivated channels, blocked channels recover through open states before closing, permitting a brief flow of resurgent Na current. Together, the reopening of channels and antagonism of inactivation can facilitate high-frequency firing. Indeed, resurgent Na current was first identified in cerebellar Purkinje neurons, which fire rapidly, and has since been described in many cell types that display fast regular spiking or burst firing (Raman and Bean, 1997; Do and Bean, 2003; Afshari et al., 2004; Cummins et al., 2005; Enomoto et al., 2006; Gittis and du Lac, 2008; Kim et al., 2010). Moreover, disruption of resurgent current correlates with abnormal motor behavior and diseases of hyperexcitability (Raman et al., 1997; Khaliq et al., 2003; Levin et al., 2006; Jarecki et al., 2010), suggesting that the presence of a blocker is a key determinant of neuronal output.

A promising candidate for the blocking protein is the Na channel auxiliary subunit $Na_V\beta4$ (scn4b), which is expressed in many brain regions where resurgent Na current is present (Yu et al., 2003). Unlike other β subunits, the cytoplasmic tail of $Na_V\beta4$ has an inserted sequence (KKLITFILKKTREK) that contains positively charged ε-amino groups and an aromatic residue, like other known Na channel blockers (Eaholtz et al., 1994). Indeed, a synthetic sequence of these amino acids ("the $\beta4$ peptide") can induce resurgent current both in Purkinje neurons with the blocker enzymatically removed and in hippocampal CA3 neurons, which lack a functional endogenous blocker (Grieco et al., 2005). The $\beta4$ peptide also rescues all phenotypes of $Na_V\beta4$ knockdown in cultured cerebellar granule neurons: it restores resurgent current amplitude and kinetics, depolarizes the inactivation curve, and increases repetitive firing (Bant and Raman, 2010).

$Na_V\beta4$, however, may not be the only endogenous blocker of Na channels. One way to aid identification of novel blocking proteins is to assess the structural requirements for open-channel block. Some features are known: altering the identity or overall number of positive charges or scrambling the sequence disrupts

Received March 21, 2011; revised June 22, 2011; accepted June 23, 2011.

Author contributions: A.H.L. and I.M.R. designed research; A.H.L. performed research; A.H.L. and I.M.R. analyzed data; A.H.L. and I.M.R. wrote the paper.

I.M.R. was supported by National Institutes of Health Grant NS39395. A.H.L. was supported by National Institutes of Health Grant T32 GM08061. We thank Dr. Andrew Dudley for sharing embryonic chicks, Dr. Ishwar Radhakrishnan for guidance on CD spectroscopy, and Dr. David Ferster for help in writing and implementing the MATLAB code for modeling. We thank Myrick Dennis of the Northwestern University Keck Biophysics Facility for technical help with CD spectroscopy. We are grateful to Raman lab members T. Aman, J. Bant, N. Zheng, M. Benton, and A. Person for helpful discussion.

Correspondence should be addressed to Dr. Indira M. Raman, Department of Neurobiology and Physiology, 2205 Tech Drive, Northwestern University, Evanston, IL 60208. E-mail: i-raman@northwestern.edu.

DOI:10.1523/JNEUROSCI.1428-11.2011

 0270-6474/11/3111527-10$15.00/0

peptide-induced resurgent current (Grieco et al., 2005). To identify other structural constraints, we have tested open-channel block by a series of peptides derived from $Na_V\beta4$ sequences in five species, as well as mutant peptides designed to disrupt residue identity and peptide structure, particularly α-helical formation. The results indicate that the essential features of $Na_V\beta4$ that produce resurgent current have been retained throughout evolution, consistent with a conserved role as a channel blocker. Moreover, the presence and relative location of a phenylalanine and two lysine residues greatly influence the stability of block, suggesting that other open-channel blocking proteins may have similar motifs.

Materials and Methods

Cell preparation. All experiments were done in accordance with guidelines approved by the Northwestern University Institutional Animal Care and Use Committee. Purkinje neurons were acutely dissociated from P14–P21 C57BL/6 mice or from late-stage embryonic (E18–E20) chick, and CA3 neurons were acutely dissociated from the hippocampus of P8–P13 mice, as in Raman and Bean (1997). Briefly, mice of either sex were anesthetized with isoflurane and rapidly decapitated; embryonic chicks of either sex were rapidly decapitated. For Purkinje cell isolation, the superficial layers of the cerebellum were removed and minced. For hippocampal cell isolation, the hippocampus was removed and slices were cut on a tissue chopper. Tissue was then incubated in warm, oxygenated dissociation solution (82 mM Na_2SO_4, 30 mM K_2SO_4, 5 mM $MgCl_2$, 10 mM HEPES, 10 mM glucose, and 0.001% phenol red, pH 7.4 with NaOH) containing 3 mg/ml protease XXIII for 7 (Purkinje) or 9 (CA3) min. Tissue was then washed and further microdissected in dissociation solution containing 1 mg/ml each of bovine serum albumin and trypsin inhibitor. Neurons were isolated by trituration in Tyrode's solution (150 mM NaCl, 4 mM KCl, 2 mM $CaCl_2$, 10 mM HEPES, 10 mM glucose, pH 7.4 with NaOH) with a series of polished Pasteur pipettes and allowed to settle in glass dishes for at least 30 min before recording. Cells were identified by their characteristic morphology; Purkinje neurons are large and teardrop-shaped, whereas CA3 neurons are pyramidal.

Electrophysiological recording and analysis. Parafilm-wrapped borosilicate pipettes (1.8–3.5 MΩ) were filled with filtered intracellular solution (108 mM $CsCH_3O_3S$, 9 mM NaCl, 1.8 mM $MgCl_2$, 0.9 mM EGTA, 9 mM HEPES, 48 mM sucrose, 4.5 mM TEACl, 4 mM MgATP, 14 mM Tris-creatine PO_4, 0.3 mM Tris-GTP, pH 7.4 with CsOH). Peptides (200 μM) synthesized by Open Biosystems were added to the intracellular solution as indicated. Drugs were purchased from Sigma-Aldrich, except for TTX (Alomone Labs). Whole-cell voltage-clamp recordings were made with an Axopatch 200B amplifier and pClamp 9.0 (Molecular Devices). Series resistance was compensated >70%. Cells were positioned in front of gravity flow pipes containing extracellular solution (150 mM NaCl, 10 mM TEACl, 10 mM HEPES, 0.3 mM $CdCl_2$, 2 mM $BaCl_2$, pH 7.4 with NaOH) ± 900 nM TTX, and subtractions isolated TTX-sensitive Na current. Data were analyzed with Igor Pro 6.0 (Wavemetrics); all means were reported as ±SEM. Statistical significance was assessed with an α level of 0.05 by either Student's two-tailed t tests or a one-way ANOVA, followed by either a planned comparison (for comparing a series of related peptides with control) or a Tukey–Kramer *post hoc* analysis (for comparing groups of related peptides with each other). To account for variance in current density, resurgent current in each cell was individually normalized to either the maximal transient current evoked at +30 mV or to the maximal resurgent current at −30 mV (as noted) before averaging. Capacitative artifacts were digitally reduced. Motif searches of the UnitProtKB/SwissProt database were performed with ScanProsite (http://ca.expasy.org/tools/scanprosite/).

Circular dichroism spectroscopy. Circular dichroism (CD) spectroscopy was done in the Northwestern University Keck Biophysics Facility, following guidelines of Kelly et al. (2005) and Greenfield (2006). Extended mouse peptide solution was prepared in 5 mM sodium phosphate (monobasic) buffer (pH 7.3) at 0.2 mg/ml. CD spectra were obtained with a 1 nm bandwidth and 1 nm step size between 260 and 185 nm on a Jasco J-815 spectropolarimeter with a 1 mm path length quartz cuvette at 23°C. The spectrum is the mean of three scans and was transformed into mean residue ellipticity from the number of residues, molecular weight, and concentration of the peptide.

Modeling. Estimation of rate constants into and out of blocked, open, and inactivated states was done in MATLAB, assuming a simple kinetic model: B ↔ O ↔ I. In this scheme, B is the blocked state, O is the open state, and I is a conglomerate of the nonconducting (inactivated or closed) states that are largely absorbing upon repolarization. Resurgent current flows as channels exit B, pass through O, and accumulate in I. Each transition rate was assigned a rate constant (k_{OB}, k_{BO}, k_{OI}, k_{IO}). The differential equations were numerically integrated and optimal rate constants were estimated for each dataset using the least-squares fitting function of MATLAB (LSQ Curvefit).

Results

Purkinje cells fire at high frequencies in many vertebrate species, including primates, cats, rodents, and fish (Thach, 1968; Latham and Paul, 1971; Häusser and Clark, 1997; Raman et al., 1997; de Ruiter et al., 2006). In mice and rats, high-frequency Purkinje cell firing depends in part on resurgent Na current (Raman et al., 1997; Khaliq et al., 2003). Although resurgent current has not yet been constituted heterologously, the best candidate for the open-channel blocking protein is the Na channel subunit $Na_V\beta4$ (Grieco et al., 2005; Bant and Raman, 2010). We reasoned that if high-frequency firing by Purkinje cells in other species also relies on resurgent current and $Na_V\beta4$-dependent open-channel block, then the structural features of $Na_V\beta4$ that permit block should likewise be conserved. However, the sequence of $Na_V\beta4$, particularly that of the cytoplasmic tail, differs among species (Fig. 1*A*). This divergence may have any one of multiple explanations. First, the few residues that are highly conserved may be sufficient for $Na_V\beta4$ to generate block. Second, the cytoplasmic tail of $Na_V\beta4$ may in fact not serve as a blocker and may have undergone significant genetic drift because of lack of selective pressure. Third, resurgent Na current may not even be present in Purkinje cells in all species, so that the sequence of $Na_V\beta4$ may be inconsequential.

To investigate the last hypothesis, we tested whether resurgent Na current is present in Purkinje cells acutely dissociated from late-stage (E18–E20) embryonic chick, in which $Na_V\beta4$ is particularly divergent from mouse. Voltage-clamped, TTX-sensitive resurgent Na currents were assayed in whole-cell recordings. Cells were first depolarized to +30 mV for 10 ms, to open channels and allow sufficient time for block, and then repolarized to potentials ranging from −90 to +20 mV for 100 ms. This "resurgent current" protocol was applied in all subsequent experiments. Resurgent current was present in all chick Purkinje cells and followed the characteristic voltage dependence seen in mouse Purkinje cells with the largest resurgent currents evoked upon repolarization to −30 mV (Fig. 1*B*). When normalized to the amplitude of the transient current evoked during the conditioning step at +30 mV, mean resurgent current amplitudes were similar between chick and mouse (chick: 8.4 ± 1.0%, $n = 12$; mouse: 10.6 ± 1.3%, $n = 7$; $p = 0.19$) (Fig. 1*C,D*). The kinetics of resurgent currents evoked at −30 mV were also indistinguishable from mouse (rise time, measured as total time to peak: chick = 4.4 ± 0.2 ms, mouse = 4.1 ± 0.2 ms, $p = 0.37$; decay time constant, τ: chick = 19.3 ± 0.9 ms, mouse = 17.5 ± 0.8 ms, $p = 0.14$; $n = 12,7$) (Fig. 1*E*).

Because resurgent current not only is present but also has similar kinetics in mouse and chick Purkinje cells, it follows that whatever the identity of the blocking protein, its function has been conserved. To provide further evidence for or against a role of $Na_V\beta4$ as a blocker, we tested whether the divergence in its sequence influenced its ability to act as a blocking protein. Previ-

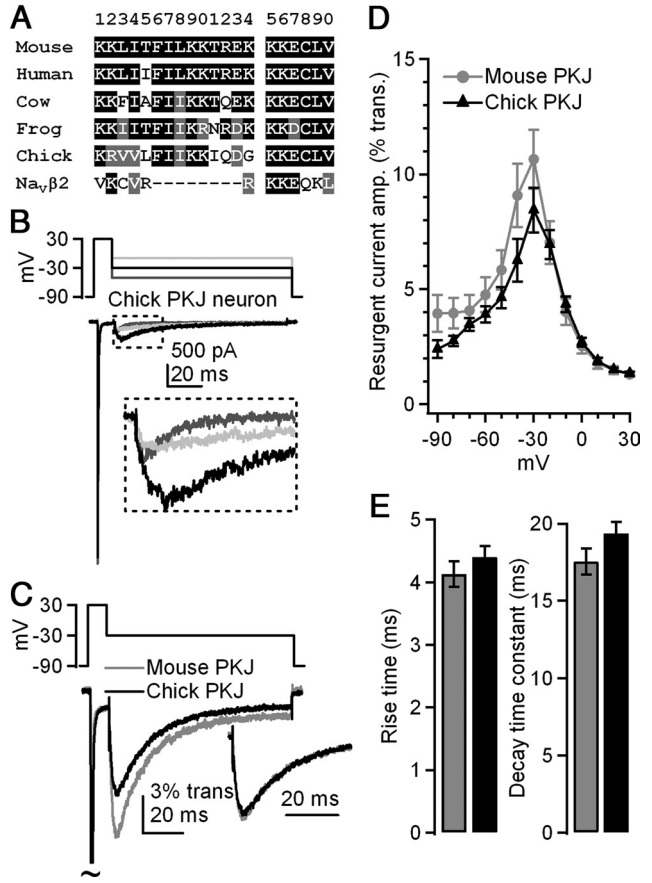

Figure 1. Purkinje neurons from embryonic chick have resurgent Na current with kinetics similar to those in mouse Purkinje neurons. ***A***, Alignment of sequences of the initial segment of the cytoplasmic tail of $Na_V\beta4$, corresponding to residues 154–173 of the mouse protein and 1–20 of the extended $\beta4$ peptide. $Na_V\beta2$ residues correspond to 151–162 of the mouse protein. Black with white lettering indicates conservation with mouse $Na_V\beta4$ sequence; gray with white lettering indicates conservative substitutions; white with black lettering indicates lack of conservation. ***B***, Top, "Resurgent current" voltage protocol, applied in all experiments. Bottom, Representative whole-cell TTX-sensitive Na currents recorded from an acutely dissociated Purkinje cell from late-stage embryonic chick (bottom). ***C***, Mean resurgent Na currents in mouse and chick Purkinje neurons, normalized to transient current evoked at +30 mV. Inset, Overlay of mean resurgent currents individually normalized to peak resurgent current. ***D***, Voltage dependence of amplitude of resurgent currents evoked by repolarization following a 10 ms step to +30 mV; amplitudes normalized to that of the transient current evoked at +30 mV. ***E***, Time to peak and decay time constant (τ) of resurgent current evoked at −30 mV. Black, chick, $n = 12$; gray, mouse, $n = 7$.

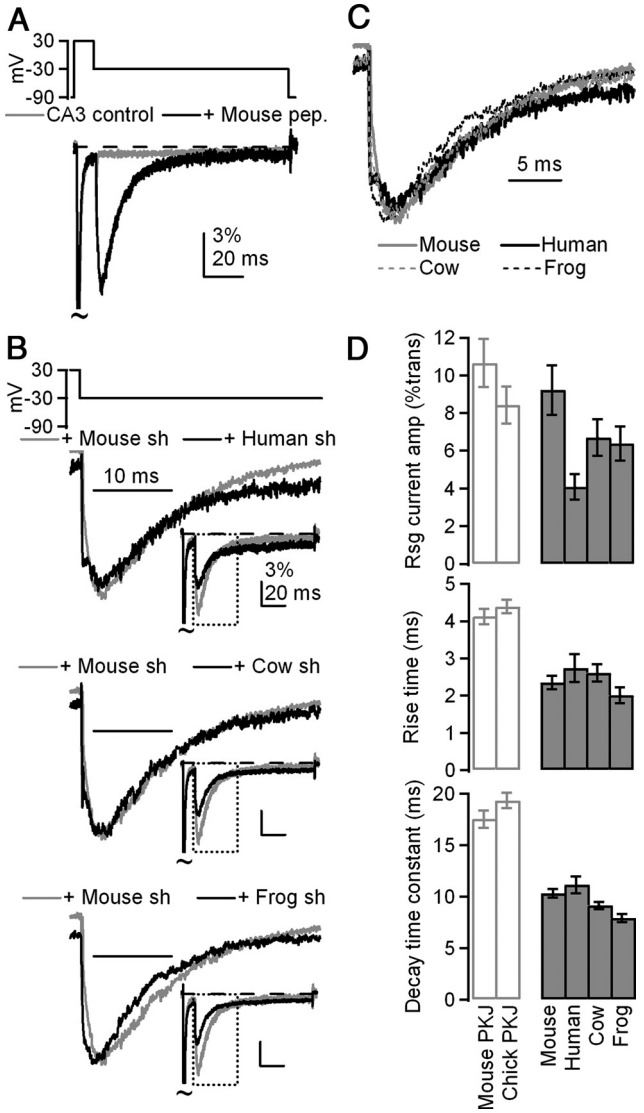

Figure 2. $\beta4$ peptides from four species evoke resurgent-like Na currents in mouse CA3 neurons. ***A***, Mean currents evoked by the resurgent current protocol (top) in dissociated mouse CA3 neurons (gray, $n = 7$), which lack endogenous block, and in CA3 neurons + 200 μM mouse $\beta4$ peptide (black, $n = 8$). Currents are normalized to transient current evoked at +30 mV. ***B***, Mean resurgent currents evoked upon repolarization to −30 mV by short (sh) $\beta4$ peptides derived from $Na_V\beta4$ sequences in various species, normalized to peak resurgent current. Insets, Currents normalized to transient current at +30 mV. Top, Human, $n = 8$; middle, cow, $n = 7$; bottom, frog, $n = 7$. ***C***, Overlay of mean resurgent currents from ***A***, normalized to peak resurgent current amplitude. ***D***, Top, Mean amplitude of resurgent current evoked at −30 mV after 10 ms conditioning step to +30 mV, normalized to transient current at +30 mV. Middle, Mean rise time of resurgent currents evoked at −30 mV. Bottom, Mean decay time constants (τ) of resurgent currents evoked at −30 mV.

ous work showed that intracellular application of a synthetic peptide comprising residues 154–167 of the cytoplasmic tail of mouse $Na_V\beta4$ can induce resurgent-like Na currents in hippocampal CA3 neurons, which lack endogenous block (Grieco et al., 2005) (Fig. 2*A*, top). We therefore assessed blocking properties of synthetic peptides derived from other $Na_V\beta4$ sequences. In this way, we used the divergence of $Na_V\beta4$ among species as a series of naturally occurring mutants to test whether key residues had been conserved. If the cytoplasmic tail of $Na_V\beta4$ directly contributes to rapid firing by physically blocking the channel, then, like the mouse $\beta4$ peptide, peptides derived from other species should be able to produce resurgent currents despite the sequence differences.

We began by studying 14-residue peptides derived from the sequences of human, cow, frog, and chick, which share between 5 and 13 amino acids with residues 154–167 of the mouse protein (Fig. 1*A*). The chick $\beta4$ peptide was initially insoluble in our internal solution, likely due to the loss of two charged and two polar residues (but see Results below). Intracellular application (200 μM) of each of the other species-derived $\beta4$ peptides, however, produced resurgent Na currents in CA3 neurons that resembled currents produced by the mouse $\beta4$ peptide (Fig. 2*A*). The mean amplitude of the resurgent current relative to transient current varied with sequence (Fig. 2*B*, insets), likely because resurgent current amplitude depends on the fraction of channels that accumulate in the blocked state during the conditioning step (Raman and Bean, 2001), which in turn depends on peptide concentration. Peptide solubility, and therefore effective concentration, varied with hydrophobicity across species, however, so

absolute amplitudes could not be taken as a good measure of the efficacy of block and unblock. When currents were instead normalized to the peak resurgent current amplitude before averaging, the similar kinetics of unblock for each peptide were readily apparent (Fig. 2*B*,*C*). Accordingly, rise time (which depends on unbinding of the blocker and is therefore a good indicator of affinity) and time constant (τ) of decay (which depends on the kinetics both of unbinding and of subsequent inactivation or deactivation of the channel) at −30 mV were used to assess the efficacy of block by a given peptide for Na channels, as these parameters are independent of concentration. Time to peak resurgent current did not vary among peptides (mouse: 2.3 ± 0.2 ms, human: 2.7 ± 0.4 ms, cow: 2.6 ± 0.2 ms, frog: 2.0 ± 0.2 ms; no significant main effect, $p = 0.32$, $7 \leq n \leq 9$) (Fig. 2*D*). Decay time constants were similar but were statistically distinguishable (mouse: 10.3 ± 0.4 ms, human: 11.1 ± 0.8 ms, cow: 9.2 ± 0.4 ms, frog: 7.9 ± 0.4 ms; significant main effect, $p = 0.002$; Tukey's *post hoc* test: $p < 0.05$ for mouse vs frog and human vs frog; $p > 0.05$ for all other comparisons, $7 \leq n \leq 9$).

Although peptide-induced resurgent current kinetics were similar among species, both the rise time and decay time constant of peptide-induced resurgent currents were faster than in Purkinje neurons (Fig. 2*D*). This difference may result in part from the different Na channel complexes in CA3 versus Purkinje neurons; as mentioned, the decay time is sensitive to the kinetics of subsequent inactivation/deactivation of the channel, which may be faster in CA3 cells, as well as to the affinity of the blocker for the α subunit, which may be lower in CA3 cells. To examine whether the short length of the peptide contributed to the apparent lower affinity for the channel, we used an extended 20-amino-acid peptide, which included the next six residues after the 14 in the original peptides. These six residues not only are highly conserved, but also contain an extra cluster of three charged residues (Fig. 1*A*). Moreover, in a previous study, the 20-mer appeared to have a slightly higher affinity for the channel (Grieco et al., 2005). Extended peptides derived from mouse, frog, and cow to include these residues slowed resurgent current kinetics compared with the short 14-mer versions (Student's *t* test, $p < 0.05$, each condition, $7 \leq n \leq 9$) (Fig. 3*A*). The extended version of the human peptide did not have significantly different kinetics, although the trend was again toward more stable block (rise time, short: 2.7 ± 0.4 ms, extended: 3.0 ± 0.3 ms, $p = 0.57$; decay τ, short: 11.1 ± 0.8 ms, extended: 12.0 ± 0.8, $p = 0.80$; $n = 8,8$). As in the case of the short peptides, the kinetics of unblock were similar for each of the extended species-derived peptides (Fig. 3*B*,*C*). Overall, the slower kinetics indicate that block by extended peptides more closely resembles that of Na channels native to Purkinje neurons (Fig. 3*A*, top, 3*C*), suggesting that at least some of the residues 168–173 are structurally important. Due to the stabilization of block by the KK(−)CLV motif, all subsequent peptides were synthesized in this extended (20-residue) form.

The addition of three charged residues was also sufficient to enable the chick $\beta4$ peptide to dissolve; importantly, this peptide indeed produced resurgent currents in CA3 cells (rise time, mouse: 5.0 ± 0.3 ms, chick: 3.7 ± 0.3 ms, $p < 0.05$; decay τ, mouse: 12.3 ± 0.6 ms, chick: 15.0 ± 1.5 ms, $p > 0.05$; $n = 9,8$). Thus, despite only sharing 11 of 20 residues, the chick $\beta4$ peptide can block Na channels much as the mouse $\beta4$ peptide does. More generally, the ability of divergent peptides to produce similar resurgent currents suggests that the residues required for open-channel block have indeed been conserved.

We next used the common elements of each sequence to identify the specific structural features that allow the cytoplasmic tail of

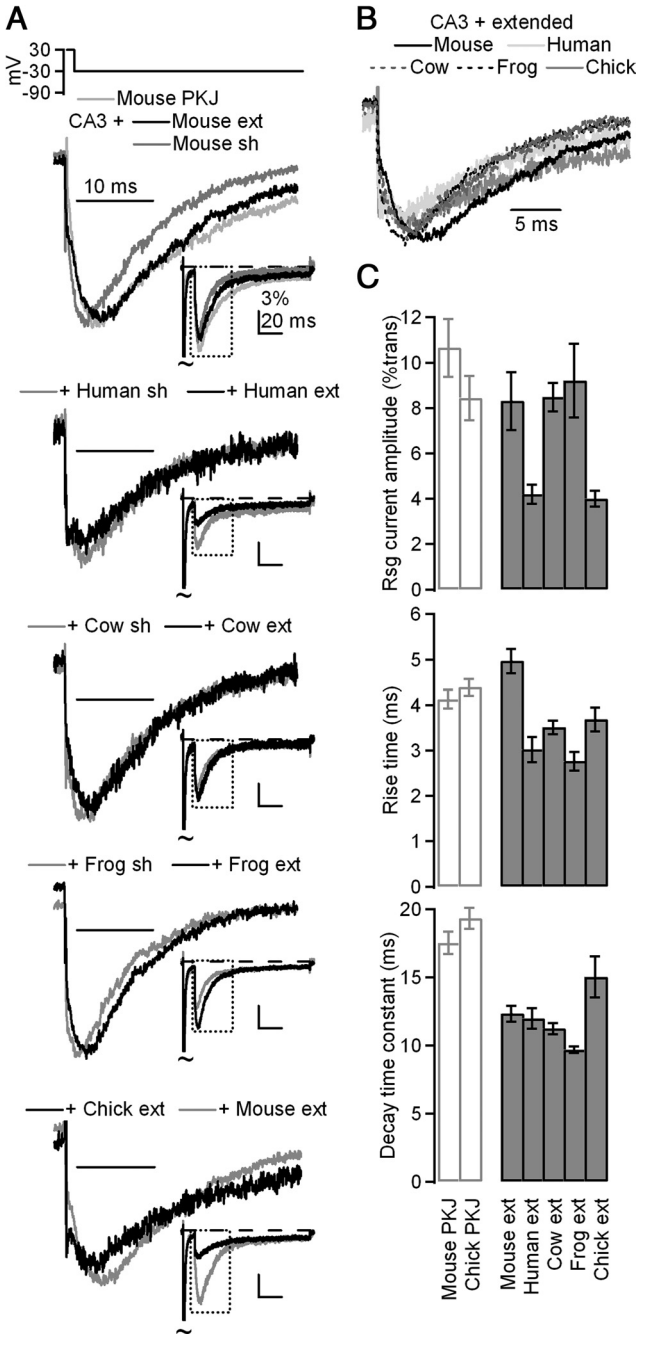

Figure 3. Extended $\beta4$ peptides in CA3 neurons induce resurgent currents with slower kinetics than short peptides. ***A***, Top, Overlay of mean currents evoked by resurgent current protocol in mouse Purkinje neurons (light gray, $n = 7$) and in CA3 neurons + 200 μM extended (ext; black, $n = 9$) or short (sh; dark gray, $n = 8$) mouse $\beta4$ peptides. Currents normalized to peak resurgent current. Middle top, Mean currents evoked in CA3 neurons with extended or short human peptide ($n = 8,8$); middle, with extended or short cow peptide ($n = 7,7$); middle bottom, with extended or short frog peptide ($n = 8,7$); bottom, with extended chick or extended mouse peptide ($n = 8,9$). Insets, Mean currents normalized to transient current at +30 mV. ***B***, Overlay of currents from ***A***, normalized to resurgent current peak. ***C***, Top, Mean amplitude of current evoked at −30 mV after 10 ms conditioning step to +30 mV, normalized to transient current at +30 mV. Middle, Mean rise time of resurgent currents evoked at −30 mV. Bottom, Mean decay time constants (τ) of resurgent currents evoked at −30 mV.

$Na_V\beta4$ to stably block Na channels. Each of the species-derived peptides shares the sequence motif K+xϕxFIϕK+xx−xKK−CLV, where + and − denote charge, ϕ is hydrophobic, and x diverges, suggesting that some subset of these residues is essential for open-

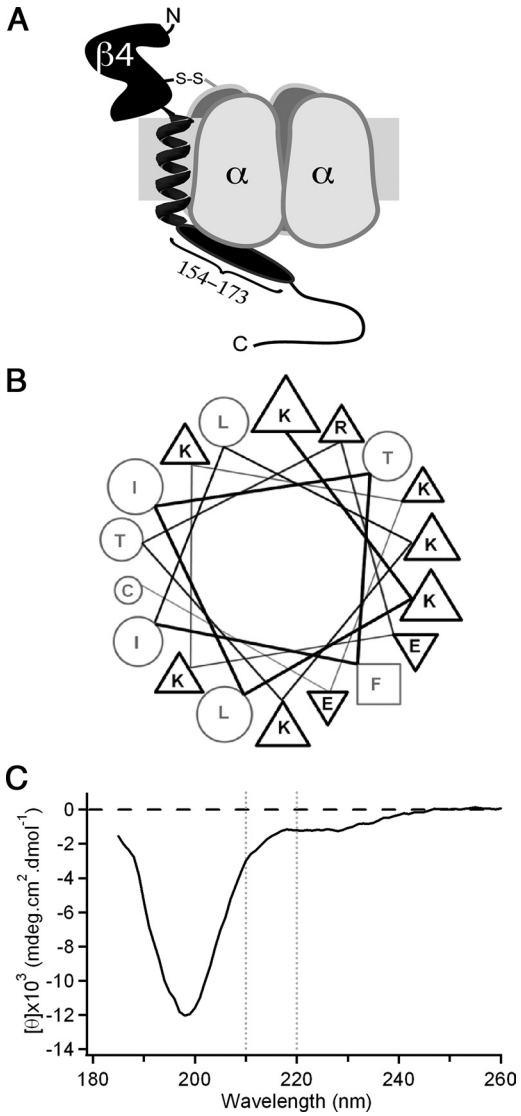

Figure 4. Possible structural conformation of the intracellular tail of $Na_V\beta4$. ***A***, Illustration of $Na_V\beta4$ (black) covalently attached to a Na channel α subunit (gray). $Na_V\beta4$ consists of a large extracellular immunoglobulin-like domain, a single transmembrane helix, and a cytoplasmic tail, the beginning of which comprises the $\beta4$ peptide (oval). ***B***, Diagram of mouse extended $\beta4$ peptide as an idealized α-helix positions the majority of the charged residues on the same face as the aromatic phenylalanine residue (square). Triangles indicate basic (up) or acidic (down) residues; circles indicate uncharged residues. ***C***, CD spectrum of extended mouse $\beta4$ peptide indicates that the sequence is largely unstructured (large minimum at ~200 nm) with a slight helical propensity (small minimum near 222 nm).

channel block (Fig. 1*A*). Moreover, given the location of the blocking sequence immediately following the transmembrane domain, how the blocker reaches the pore and what structure it adopts remain open questions (Fig. 4*A*). A possible hint comes from the pattern of conserved residues every three to four amino acids (K2, F6, K9). If the sequence assumed an α-helical structure, the hydrophobic and charged residues would be separated and the aromatic phenylalanine would align with charged lysine residues to form a potential interface for binding to the channel pore (Fig. 4*B*). Secondary structure, however, is often influenced by local as well as long-range interactions and, in the absence of the latter, free peptides may sample many different conformations.

Nevertheless, some peptides indeed assume a helical conformation, albeit with a low probability, even when free in solution (Cusdin et al., 2010). We therefore used CD spectroscopy to test for potential secondary structure in the extended mouse $\beta4$ peptide (Fig. 4*C*). The spectrum suggests, however, that despite the presence of some negative ellipticity at wavelengths >210 nm and a shallow minimum near 222 nm, reflecting a slight propensity for α-helical conformation, the peptide is largely unstructured, indicated by a deep minimum at 198 nm that is characteristic of "random coil" conformations (Kelly et al., 2005; Greenfield, 2006). One interpretation of this result is that the $\beta4$ peptide, like many short peptides, lacks a stable structure simply because it has been isolated from the rest of the protein; alternatively, the cytoplasmic tail of even the intact $Na_V\beta4$ may in fact be intrinsically unstructured and conformationally flexible. In either case, the blocking sequence may assume a well defined secondary structure only on interaction with its binding site on the α subunit. We therefore sought ways to investigate the structure of the peptide when bound to its target, as well as to identify which residues of the peptide participate in this interaction.

To do so, we generated three mutant peptides from the mouse $\beta4$ sequence. Because the phenylalanine is completely conserved, we hypothesized that it might play a particularly important role in stabilizing open-channel block. We therefore generated a peptide from the mouse $Na_V\beta4$ sequence in which the phenylalanine had been substituted with the nonaromatic alanine. This peptide (F6A) consistently produced currents upon repolarization, indicating that the loss of the phenylalanine did not prevent the peptide from blocking open channels during the conditioning step; however, both the time to peak and decay time constant were significantly faster than that produced by the control peptide, indicating that mutant peptide had greatly reduced affinity for the pore upon repolarization (rise time: 1.2 ± 0.2 ms, $p < 0.001$; decay τ: 5.4 ± 0.4 ms, $p < 0.001$; $n = 7$) (Fig. 5*A*, top, 5*B*,*C*).

Next, based on the likely role of the phenylalanine in stabilizing open-channel block, we explored the hypothesis that the peptide forms an α-helix by switching the locations of F6 and L8, such that the phenylalanine protrudes from the other side of a putative helix (F6L/L8F). Like F6A, F6L/L8F blocked open channels upon depolarization but unbound more rapidly than the mouse peptide upon repolarization (rise time: 1.9 ± 0.2 ms, $p < 0.001$; decay τ: 8.8 ± 0.5 ms, $p < 0.001$; $n = 9$) (Fig. 5*A*, middle, 5*B*,*C*).

Last, because prolines can disrupt α-helices due to the lack of an amide hydrogen (e.g., Cusdin et al., 2010), we disrupted the relative position of the phenylalanine and the highly conserved lysine side chains by substituting a proline for a leucine residue between F6 and K9/K10 (L8P). Like F6A and F6L/L8F, this peptide blocked open channels during the conditioning step, but unblocked rapidly upon repolarization (rise time: 0.6 ± 0.1 ms, $p < 0.001$; decay τ: 5.9 ± 0.6 ms, $p < 0.001$; $n = 9$) (Fig. 5*A*, bottom, 5*B*,*C*). Notably, all three of the mutant peptides that disrupted the presence and relative position of the phenylalanine residue differed from the control mouse peptide to a far greater extent than did any of the naturally occurring variants across species. Together, the faster kinetics of the repolarization-evoked currents produced by these mutant peptides support a role of the phenylalanine residue in stabilizing block at negative voltages, which generates the slow rise time associated with endogenous resurgent current, either directly by interacting with the channel pore or indirectly by enforcing a helical structure to properly position other residues.

We next investigated whether other highly conserved residues, particularly charged residues, might also be necessary for either producing block or permitting unblock. We therefore

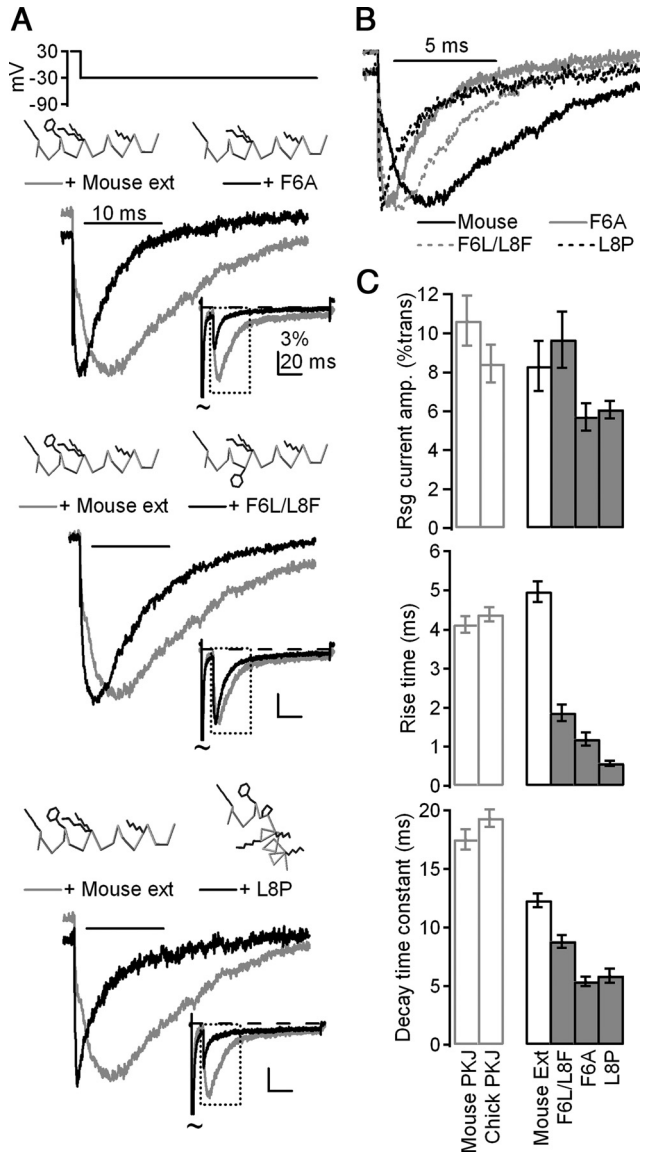

Figure 5. The identities and orientation of a phenylalanine and two lysine residues are key determinants of resurgent current kinetics. ***A***, Mean currents evoked by the resurgent current protocol in CA3 neurons with control mouse (gray) and mutant (black) $\beta4$ peptides, normalized to peak current evoked by repolarization. Top, F6A, $n = 7$; middle, F6A/L8F, $n = 9$; bottom, L8P, $n = 9$. Insets, Mean currents normalized to peak transient current at +30 mV. Peptide schematics were rendered in Deepview (Swiss Institute of Bioinformatics). Gray indicates α carbon trace; black indicates side chains of K2, F6, K9, K10, and K16. Other side chains are blanked for clarity. ***B***, Overlay of mean currents from ***A***, normalized to resurgent current peak. ***C***, Top, Mean amplitude of currents evoked at −30 mV after 10 ms conditioning step to +30 mV, normalized to transient current at +30 mV. Middle, Mean rise time of resurgent currents evoked at −30 mV. Bottom, Mean decay time constants (τ) of resurgent currents evoked at −30 mV.

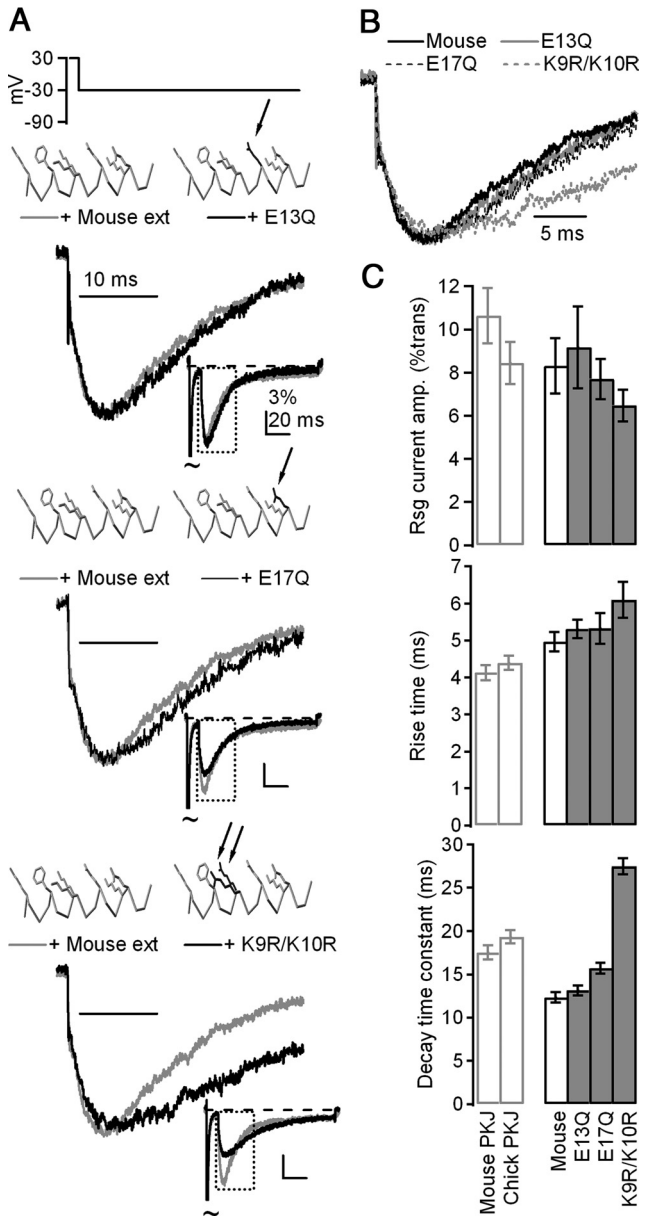

Figure 6. Mutations of basic residues, but not acidic residues, alter the affinity of $\beta4$ peptides for Na channels. ***A***, Mean currents evoked by resurgent current protocol in CA3 neurons with control mouse (gray) and mutant (black) $\beta4$ peptides, normalized to peak current evoked upon repolarization. Top, E13Q, $n = 9$; middle, E17Q, $n = 7$; bottom, K9R/K10R, $n = 8$. Insets, Mean currents normalized to peak transient current at +30 mV. Peptide schematics were rendered in Deepview (Swiss Institute of Bioinformatics). Gray indicates α carbon trace and control side chains (K2, F6, K9, K10, E13, K16, E17; others blanked for clarity). Black indicates side chains that deviate from control. ***B***, Overlay of currents from ***A***, normalized to resurgent current peak. ***C***, Top, Mean amplitude of currents evoked at −30 mV after 10 ms conditioning step to +30 mV, normalized to transient current at +30 mV. Middle, Mean rise time of resurgent currents evoked at −30 mV. Bottom, Mean decay time constants (τ) of resurgent currents evoked at −30 mV.

tested the role of two lysines that follow the phenylalanine (K9 and K10) by substitution to arginine. Previous experiments demonstrated that neutralization of these two lysines prevents open-channel block, whereas conversion of all five lysines in the short peptide to arginine produces stable block at all potentials that reverses only upon washout (Grieco et al., 2005). In contrast, the more conservative substitution of just two arginines (K9R/K10R) stabilized block relative to the mouse $\beta4$ peptide but still permitted expulsion upon repolarization, producing currents upon repolarization with slower kinetics than the extended mouse peptide (rise time: 6.1 ± 0.5 ms, $p = 0.051$; decay τ: 27.5 ± 0.9 ms, $p < 0.001$; $n = 8$) (Fig. 6*A*, top, 6*B*,*C*).

In addition to aromatic (F) and basic (K/R) residues, two acidic residues (E13 and E17) are also highly conserved among species (Fig. 1*A*). To investigate a potential role for their negative charges in producing and/or stabilizing block, we tested the effect of peptides in which the glutamate had been substituted with glutamine (to preserve size and polarity, but not charge). Unlike

other mutant peptides, which altered the affinity of $\beta4$ peptides for the Na channel, the glutamine-substituted peptides produced resurgent current with kinetics that were indistinguishable from those produced by the mouse $\beta4$ peptide (E13Q: $n = 9$, rise time $= 5.3 \pm 0.2$ ms, $p = 0.36$; decay $\tau = 13.1 \pm 0.5$ ms, $p = 0.34$; E17Q: $n = 7$, rise time $= 5.3 \pm 0.4$ ms, $p = 0.47$; decay $\tau = 15.7 \pm 0.6$ ms, $p < 0.01$) (E13Q: Fig. 6*A*, middle, 6*B*,*C*; E17Q: Fig. 6*A*, bottom, 6*B*,*C*). Thus, unlike the basic residues, the charge on the acidic residues did not have a measurable influence on open-channel block. The functional groups on the basic residues, however, may directly set the stability of $\beta4$ peptide block of Na channels.

Together, the combination of CD spectroscopy and electrophysiology with the mutant peptides bring up a scenario that could resolve the question of how the sequence corresponding to the $\beta4$ peptide, which immediately follows the (presumed) α-helical transmembrane segment, could gain access to the pore of the α subunit. If, when the channel is closed, the intracellular tail is free to sample many conformations, then, upon channel opening, its flexibility may allow it to find its exposed binding site. Binding may drive the equilibrium between conformations to favor a well defined, likely α-helical conformation of the peptide, as the phenylalanine and lysine residues interact with the binding site and block the permeation pathway. When these residues are absent or altered, the affinity of this sequence for its binding site is lower, facilitating unblock and producing faster resurgent currents. Similarly, when the presence of a rigid proline residue constrains the conformation, affinity is likewise lower.

Although this question cannot be answered fully in the absence of further structural information, the voltage dependence of peptide-induced resurgent currents provides further support for variability in peptide affinity as a function of these residues. As mentioned, resurgent current amplitude depends both on the rate of unblock, which is affected by inwardly permeating Na ions that displace the blocker (Aman and Raman, 2010), as well as on total open time, which is determined by the relative rates of entry into inactivated or closed (deactivated) states. In Purkinje cells, resurgent current is maximal at −30 mV (Fig. 7*A*, left): amplitudes fall off steeply at more depolarized potentials because the lower driving force is not sufficient to allow Na to displace the blocker easily; amplitudes fall off steeply at more negative potentials because after unblocking, channels deactivate too quickly to pass much current (Raman and Bean, 2001; Afshari et al., 2004; Aman and Raman, 2010).

In CA3 neurons, the wild-type mouse peptide also produces resurgent currents that are maximal at −30 mV; however, the difference between −30 mV and more depolarized potentials is smaller (Fig. 7*A*, left). This effect is consistent with the slightly reduced affinity measured by kinetics, as the blocker is more readily displaced even where the driving force is lower. This effect is even greater with mutant peptides that produce less stable block (F6A and F6L/L8F), such that the voltage dependence is shifted and the largest currents are evoked upon repolarization to −20 mV (Fig. 7*A*, right). In the extreme case of L8P, where unblock is almost instantaneous, the voltage dependence resembles that of a tail current whose amplitude follows that of the driving force.

Although it is likely that mutating the peptide modifies its affinity for the channel, it is also possible that the presence of the peptides directly influences binding by the inactivation gate. To estimate the extent to which the changes in resurgent current kinetics can be attributed to modifications in affinity alone, we implemented a simplified kinetic model that described the shape

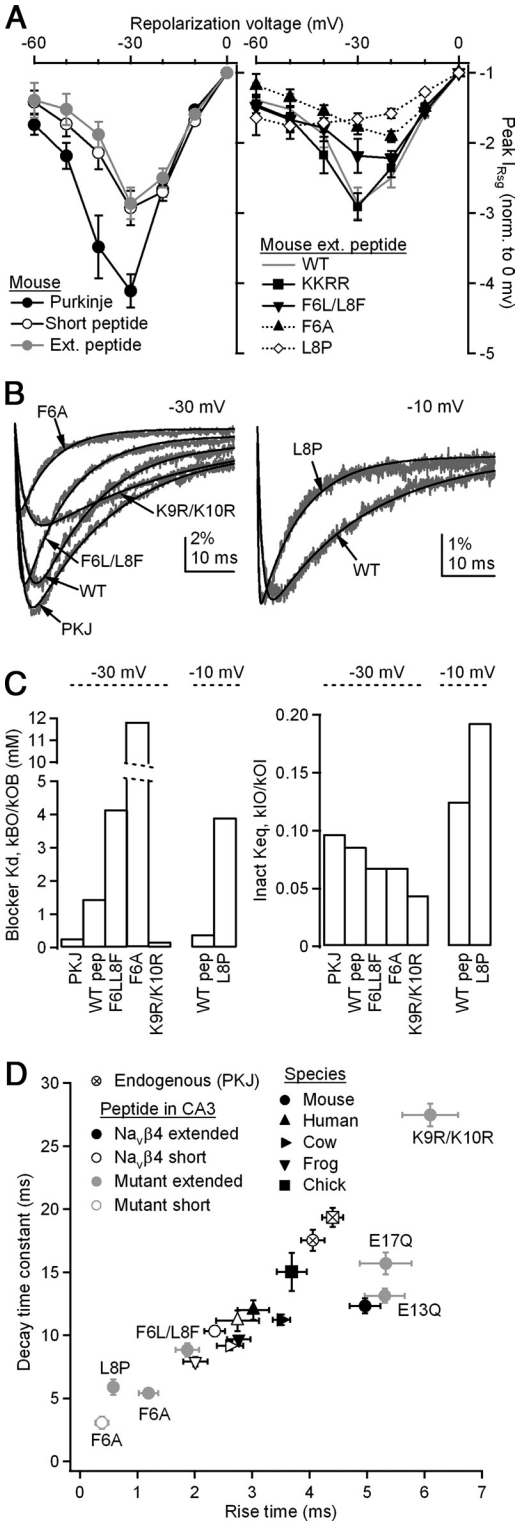

Figure 7. Kinetics of endogenous resurgent Na current are more closely replicated by $\beta4$ peptides derived from various species than by mutant peptides. ***A***, Voltage dependence of resurgent currents in mouse and chick Purkinje neurons and mouse CA3 neurons with various $\beta4$ peptides. All currents were evoked by repolarization to indicated voltage for 100 ms following a 10 ms conditioning step to +30 mV and are normalized to the peak resurgent current evoked at 0 mV; $7 \leq n \leq 12$. Error bars indicate ±SEM. ***B***, Mean resurgent currents (gray) and fits (black), at −30 mV (left) and at −10 mV (right). ***C***, Left, Blocker K_d obtained from fits by ratio of BO rate to OB rate, corrected for concentration of 200 μM. Right, K_{eq} of inactivation, calculated from ratio of the rate of IO to that of OI. ***D***, Kinetics of resurgent Na currents. Currents evoked as in ***A***. *x*-axis, time to peak resurgent current from onset of voltage step; *y*-axis, decay time constant (τ) of resurgent current, fit with a single exponential.

Table 1. Rate constants of fits to native and peptide-induced resurgent current

	k_{BO} (s^{-1})	k_{OB} (s^{-1})	k_{OI} (s^{-1})	k_{IO} (s^{-1})
−30 mV				
Purkinje (native)	576	207	72	7
Wild-type (peptide)	449	62	88	8
F6L/L8F	1334	64	107	7
F6A	2458	42	147	10
K9R/K10R	232	265	68	3
−10 mV				
Wild-type	742	370	70	8
L8P	4930	252	109	21

of the resurgent current as a transition from a blocked state B, through an open state O, to a nonconducting but unblocked state I, which includes both inactivated states (from fast inactivation) and closed states (from deactivation). Forward rates were given as k_{BO} and k_{OI}, and back rates were given as k_{OB} and k_{IO}. Also for simplicity, just before repolarization, the blocked state was assumed to be completely occupied. Curve fitting permitted an estimation of the four rates. Because the wild-type and mutant peptides were approximately equally soluble, we assumed a 200 μM concentration, from which a measure of the affinity of the blocker was obtained from the dissociation constant (K_d), k_{BO}/k_{OB}, and a measure of the stability of the inactivated state was obtained from the equilibrium constant (K_{eq}), k_{IO}/k_{OI}. A similar measurement was made for the data from mouse Purkinje cells. Based on Grieco et al. (2005), the concentration of the endogenous blocker was estimated at 100 μM. Mean resurgent currents for each peptide and the corresponding fits are displayed in Figure 7*B*. Rate constants are given in Table 1. At −30 mV, the K_d of the blocker was 0.28 mM for Purkinje neurons and 1.46 mM for the extended mouse $\beta4$ peptide in CA3 neurons. As predicted, the affinity was much lower for mutant peptides: 4.15 mM for F6L/L8F and 11.82 mM for F6A. Conversely, the affinity was higher for K9R/K10R: 0.18 mM. Interestingly, this value is close to the concentration of the peptide, indicating that at −30 mV, the rates of block and unblock are approximately equal.

Initial fits to the mean L8P current did not converge well, likely because block by L8P is particularly unstable; as suggested by Figure 7*A*, repolarization to more negative potentials elicited a particularly rapid unblock, evoking a tail-like current. The rapid rise provided too few points for an accurate fit at −30 mV. Therefore, we instead fit L8P, as well as wild-type peptide for comparison, at −10 mV, where the rise time is slower. At this voltage, both datasets were well fit by the model. The estimated K_d for the wild-type peptide at −10 mV was 0.4 mM, threefold higher than at −30 mV, consistent with a higher affinity block in the face of fewer permeating ions when the driving force is reduced. In contrast, the affinity of L8P was 3.91 mM at −10 mV. This 10-fold decrease in affinity supports the hypothesis that the proline indeed disrupts binding.

Unlike the threefold to 10-fold differences in the affinity for the blocked state, the peptides produced relatively small changes in the rates into and out of the inactivated (or closed) state (Fig. 7*C*, right). The ratio k_{IO}/k_{OI} was 0.086 in control at −30 mV and remained near this value in most peptides (F6A, 0.068; F6LL8F, 0.068; K9R/K10R, 0.044; at −10 mV, the control ratio was 0.13 and L8P was 0.19). Thus, although it remains possible that the mutations in the peptides also directly influence the transition rates between open and inactivated (or closed) states, changes in the stability of open-channel block can account for most of the observed changes in resurgent current kinetics.

Thus, both the time to peak and decay rate of resurgent current reflect affinity. To look at the covariance in these two measures across all peptides, we plotted them in Figure 7*D*. As expected, the two variables were tightly correlated ($R^2 = 0.75$). Moreover, the summary plot reveals clustering of different groups of peptides. Resurgent Na currents evoked by those derived from the various animal species, particularly the extended peptides, most closely replicate the kinetics of resurgent currents endogenous to Purkinje cells, consistent with the idea that this portion of the $Na_V\beta4$ tail is well suited as a blocking protein of voltage-gated Na channels across vertebrate species. In contrast, mutant peptides with the identity or orientation of the F6 disrupted generate unphysiologically fast resurgent kinetics, whereas peptides with K9 and K10 replaced by arginine residues yield unusually slow kinetics. Substituting either E13 or E17 with a glutamine residue does not alter resurgent current kinetics. Thus, the physiological affinity of the peptide for the channel is primarily dependent on the highly conserved phenylalanine and two lysines separated by approximately one turn of an α-helix.

Discussion

These data indicate that despite the divergence of $Na_V\beta4$ across species, the structural elements required for resurgent Na current remain intact. Mutating the $\beta4$ peptide demonstrates that the identities and relative orientation of a highly conserved phenylalanine and at least two conserved lysines are key determinants of how strongly $\beta4$ peptides interact with the Na channel pore. Open-channel block is required for resurgent current (Raman and Bean, 2001; Khaliq et al., 2003), which in turn is required for the rapid firing that is typical of vertebrate Purkinje cells (Pugh and Raman, 2009). Therefore, the simplest interpretation is that the adaptive significance of rapid firing has exerted a selective pressure across species, which has retained the residues that facilitate a physiological blocking action by the cytoplasmic tail of $Na_V\beta4$. Nevertheless, because most proteins exist in multiple isoforms, it is unlikely that $Na_V\beta4$ is the only endogenous blocking protein in the nervous system. Therefore, the data on the structural requirements for a resurgent-current-producing block provide guidelines for identification of additional Na channel blockers.

Resurgent current in different species

Purkinje cells isolated from embryonic chick produce resurgent current, making this species the fourth in which resurgent current has been recorded, along with rat, mouse, and electric fish (Raman and Bean, 1997; Raman et al., 1997; de Ruiter et al., 2006). In addition, five different $\beta4$ peptides, representing at least 13 species [mouse/rat, human/chimpanzee/marmoset/orangutan/gibbon, cow/panda/wild boar, frog (*Xenopus tropicalis* and *X. laevis*), and chick], can induce resurgent current in neurons that lack an endogenous open-channel blocking protein. Dog, zebra finch, horse, opossum, turkey, anole, and zebrafish brain also share the motif K+$\phi\phi$xF$\phi\phi$K+xx−xKK−CLV, with the exception of substitutions K2N and K9A in the zebrafish. The retention of key amino acids suggests that peptides from these species may also produce open-channel block. The kinetics of unblock do differ slightly among the species-derived peptides tested; the frog peptide produces faster resurgent currents than the others. Although it is possible that each $Na_V\beta4$ sequence is tailored to the corresponding α subunits, so that testing block in mouse neurons highlights species mismatches, the high conservation of α subunits across species makes this interpretation unlikely. For example, $Na_V1.6$, the primary carrier of resurgent

current in Purkinje cells (Raman et al., 1997), is 95% conserved between mouse and chick; conversely, $Na_V\beta4$ is only 58% conserved. Alternatively, differences may be physiological. In this study, all kinetics were measured at 22°C, whereas body temperature varies across species. Interestingly, the frog, which has the lowest body temperature, had the peptide that produced the fastest kinetics at 22°C.

Role of the α subunit

In contrast to the moderate cross-species variability, peptide-induced current in CA3 neurons was significantly faster than endogenous current in Purkinje neurons. Differences were evident both in the rise time, which reflects the affinity of the blocker, and in the decay time, which depends not only on the unblocking rate but also on inactivation and deactivation rates of the α subunit. A likely explanation for the faster kinetics in CA3 cells is the composition of the Na channel complexes. Although both cell types express $Na_V1.2$ and $Na_V1.6$ subunits, only Purkinje cells express $Na_V1.1$ (Felts et al., 1997; Schaller and Caldwell, 2003). Open-channel block is indeed sensitive to α subunit identity: loss of $Na_v1.6$ expression slows the decay time constant of resurgent Na current by >50% in Purkinje neurons (Aman and Raman, 2007; Kalume et al., 2007). Likewise, in cerebellar nuclear and subthalamic nuclear neurons, in which normal resurgent current does not require $Na_V1.6$, the kinetics are slower than in Purkinje cells (Do and Bean, 2004; Aman and Raman, 2007), suggesting that the blocking protein binds more tightly to $Na_V1.1$ than to $Na_V1.6$. Thus, the tendency toward faster kinetics of peptide-induced resurgent current may reflect an abundance of $Na_V1.6$ and lack of $Na_V1.1$ in CA3 cells.

In addition, other proteins may regulate the availability of open channels, thus influencing open-channel block. Indeed, slower inactivation rates and larger persistent currents are favored by $Na_V\beta2$ or $Na_V\beta4$ and antagonized by $Na_V\beta1$ (Aman et al., 2009). Because CA3 neurons do not naturally produce resurgent current, their Na channels complexes may lack protein–protein interactions that facilitate and/or stabilize open-channel block.

Key residues involved in open-channel block

The present data further support the validity of the approach of using the $\beta4$ peptide to mimic endogenous block (Kim et al., 2010; Theile et al., 2011); they also suggest, however, that 20-residue $\beta4$ peptides, which stabilize the binding of the peptide, may better replicate the kinetics of native resurgent current. Not all residues in the $\beta4$ peptide play an equivalent role in generating open-channel block, however. For example, R12 in mouse is Q12 in cow and chick, whereas mouse T5 is I5, A5, or L5 in other species, suggesting that charge and polarity of these residues can vary widely with little effect on peptide-induced resurgent currents. Even conserved sites need not participate in block as neutralizing the charges on E13 and E17 was without effect. In contrast, the identities of F6 and K9/K10 residues are tightly linked to blocking kinetics. Interestingly, phenylalanine and lysine residues can participate in cation–π interactions; such interactions contribute to use-dependent local anesthetic block (Ahern et al., 2008). Perhaps a related point is that heterologously expressed cardiac Na channels lose their susceptibility to block by the (mouse) $\beta4$ peptide when a phenylalanine residue in the local anesthetic binding site in DIV S6 is mutated, raising the possibility that this region of the α subunit interacts directly with the blocker (Wang et al., 2006). Moreover, the stability of block is sensitive to the relative orientation of F6 and K9/K10, consistent with the peptide, and by extension the initial cytoplasmic segment of full-length $Na_V\beta4$, assuming an α-helical conformation, at least on interaction with its binding site.

Potential diversity of blocking proteins

The link between $Na_V\beta4$ and resurgent current is still being defined. Although siRNA-mediated knockdown of $Na_V\beta4$ can abolish resurgent current in cultured granule neurons (Bant and Raman, 2010), coexpressing $Na_V\beta4$ and neuronal α subunits in HEK cells cannot reproduce resurgent Na current (Chen et al., 2008; Aman et al., 2009; Theile et al., 2011). The failure of heterologous expression systems to reconstitute resurgent current suggests that the behavior of $Na_V\beta4$ depends on aspects of the cellular environment, such as expression of auxiliary proteins or phosphorylation state (Grieco et al., 2002). Conversely, in neurons with native resurgent current, whether the endogenous blocker is $Na_V\beta4$ or another protein may depend on the cell. Indeed, the overlap between expression of $Na_V\beta4$ and incidence of resurgent current is broad but incomplete: neurons in the cerebellum, brainstem, subthalamic nuclei, and dorsal root ganglia express resurgent current as well as $Na_V\beta4$ (Yu et al., 2003), whereas some hippocampal and globus pallidus neurons have resurgent current but low $Na_V\beta4$ expression, assayed by *in situ* hybridizations (Yu et al., 2003; Castelli et al., 2007; Mercer et al., 2007). The low signal need not indicate a lack of protein expression, however, because cerebellar granule cells also show little mRNA expression in *in situ* hybridizations but mRNA is evident when assayed by quantitative PCR (Bant and Raman, 2010).

Nevertheless, the imperfect overlap of $Na_V\beta4$ and resurgent current raises the possibility that distinct proteins produce endogenous open-channel block in some neurons, motivating searches for candidate proteins that share motifs with the cytoplasmic tail of $Na_V\beta4$ and might be alternative Na channel blockers. Based on the constraints defined by conservation across species, using ScanProsite (de Castro et al., 2006) to scan for proteins in UniProtKB/Swiss-Prot (*Mus musculus*) that contain K+xxxF$\phi\phi$K+ yields only $Na_V\beta4$ and a histone acetyltransferase (MYST4), which, as a nuclear protein, is unlikely to be a channel blocker. However, including only those residues confirmed as necessary to generate resurgent Na current with normal kinetics yields many more proteins. For example, 4718 mouse proteins contain the motif Fxx++ (where x cannot be proline). Constraining sites 2 and 3 of this motif to be hydrophobic limits the candidates to 610 proteins. Proteins on this list that potentially interact with Na channels, and in which the relevant sequence is intracellular, may ultimately become good candidates for novel blocking proteins.

The present data suggest, however, that efficacy of block is likely to vary according to sequence. In fact, even slight alterations in the stability of block may have physiological implications. If a blocking protein interacts only weakly with the channel pore (as in peptides in which F6 was manipulated), it may not sufficiently prevent Na channels from accumulating in inactivated states during repetitive firing. Consistent with this idea, in BACE1−/− Purkinje neurons, the affinity of the blocker relative to the inactivation gate is reduced, correlating with reduced spontaneous firing frequencies (Huth et al., 2011). Alternatively, if a blocking protein interacts unusually strongly with the channel pore, it may not be readily expelled upon repolarization, thereby reducing interspike Na currents. Thus, if multiple endogenous blocking proteins exist, they may contribute to generating a diversity of resurgent current kinetics, facilitating a variety of firing patterns in different neurons.

References

Afshari FS, Ptak K, Khaliq ZM, Grieco TM, Slater NT, McCrimmon DR, Raman IM (2004) Resurgent Na currents in four classes of neurons of the cerebellum. J Neurophys 92:2831–2843.

Ahern CA, Eastwood AL, Dougherty DA, Horn R (2008) Electrostatic contributions of aromatic residues in the local anesthetic receptor of voltage-gated sodium channels. Circ Res 102:86–94.

Aman TK, Raman IM (2007) Subunit dependence of Na channel slow inactivation and open channel block in cerebellar neurons. Biophys J 92:1938–1951.

Aman TK, Raman IM (2010) Inwardly permeating Na ions generate the voltage dependence of resurgent Na current in cerebellar Purkinje neurons. J Neurosci 30:5629–5634.

Aman TK, Grieco-Calub TM, Chen C, Rusconi R, Slat EA, Isom LL, Raman IM (2009) Regulation of persistent Na current by interactions between β subunits of voltage-gated Na channels. J Neurosci 29:2027–2042.

Bant JS, Raman IM (2010) Control of transient, resurgent, and persistent current by open-channel block by Na channel beta4 in cultured cerebellar granule neurons. Proc Natl Acad Sci U S A 107:12357–12362.

Castelli L, Nigro MJ, Magistretti J (2007) Analysis of resurgent sodium-current expression in rat parahippocampal cortices and hippocampal formation. Brain Res 1163:44–55.

Chen Y, Yu FH, Sharp EM, Beacham D, Scheuer T, Catterall WA (2008) Functional properties and differential neuromodulation of Na(v)1.6 channels. Mol Cell Neurosci 38:607–615.

Cummins TR, Dib-Hajj SD, Herzog RI, Waxman SG (2005) Nav1.6 channels generate resurgent sodium currents in spinal sensory neurons. FEBS Lett 579:2166–2170.

Cusdin FS, Nietlispach D, Maman J, Dale TJ, Powell AJ, Clare JJ, Jackson AP (2010) The sodium channel {beta}3-subunit induces multiphasic gating in NaV1.3 and affects fast inactivation via distinct intracellular regions. J Biol Chem 285:33404–33412.

de Castro E, Sigrist CJ, Gattiker A, Bulliard V, Langendijk-Genevaux PS, Gasteiger E, Bairoch A, Hulo N (2006) ScanProsite: detection of PROSITE signature matches and ProRule-associated functional and structural residues in proteins. Nucleic Acids Res 34:W362–W365.

de Ruiter MM, De Zeeuw CI, Hansel C (2006) Voltage-gated sodium channels in cerebellar Purkinje cells of mormyrid fish. J Neurophysiol 96:378–390.

Do MT, Bean BP (2003) Subthreshold sodium currents and pacemaking of subthalamic neurons: modulation by slow inactivation. Neuron 39:109–120.

Do MT, Bean BP (2004) Sodium currents in subthalamic nucleus neurons from Nav1.6-null mice. J Neurophysiol 92:726–733.

Eaholtz G, Scheuer T, Catterall WA (1994) Restoration of inactivation and block of open sodium channels by an inactivation gate peptide. Neuron 12:1041–1048.

Enomoto A, Han JM, Hsiao CF, Wu N, Chandler SH (2006) Participation of sodium currents in burst generation and control of membrane excitability in mesencephalic trigeminal neurons. J Neurosci 26:3412–3422.

Felts PA, Yokoyama S, Dib-Hajj S, Black JA, Waxman SG (1997) Sodium channel alpha-subunit mRNAs I, II, III, NaG, Na6 and hNE (PN1): different expression patterns in developing rat nervous system. Brain Res Mol Brain Res 45:71–82.

Gittis AH, du Lac S (2008) Similar properties of transient, persistent, and resurgent Na currents in GABAergic and non-GABAergic vestibular nucleus neurons. J Neurophysiol 99:2060–2065.

Greenfield NJ (2006) Using circular dichroism spectra to estimate protein secondary structure. Nat Protoc 1:2876–2890.

Grieco TM, Afshari FS, Raman IM (2002) A role for phosphorylation in the maintenance of resurgent sodium current in cerebellar Purkinje neurons. J Neurosci 22:3100–3107.

Grieco TM, Malhotra JD, Chen C, Isom LL, Raman IM (2005) Open-channel block by the cytoplasmic tail of sodium channel $\beta4$ as a mechanism for resurgent sodium current. Neuron 45:233–244.

Häusser M, Clark BA (1997) Tonic synaptic inhibition modulates neuronal output pattern and spatiotemporal synaptic integration. Neuron 19:665–678.

Huth T, Rittger A, Saftig P, Alzheimer C (2011) β-Site APP-cleaving enzyme 1 (BACE1) cleaves cerebellar Na+ channel $\beta4$-subunit and promotes Purkinje cell firing by slowing the decay of resurgent Na+ current. Pflugers Arch 461:355–371.

Jarecki BW, Piekarz AD, Jackson JO 2nd, Cummins TR (2010) Human voltage-gated sodium channel mutations that cause inherited neuronal and muscle channelopathies increase resurgent sodium currents. J Clin Invest 120:369–378.

Kalume F, Yu FH, Westenbroek RE, Scheuer T, Catterall WA (2007) Reduced sodium current in Purkinje neurons from Nav1.1 mutant mice: implications for ataxia in severe myoclonic epilepsy in infancy. J Neurosci 27:11065–11074.

Kelly SM, Jess TJ, Price NC (2005) How to study proteins by circular dichroism. Biochim Biophys Acta 1751:119–139.

Khaliq ZM, Gouwens NW, Raman IM (2003) The contribution of resurgent sodium current to high-frequency firing in Purkinje neurons: an experimental and modeling study. J Neurosci 23:4899–4912.

Kim JH, Kushmerick C, von Gersdorff H (2010) Presynaptic resurgent Na+ currents sculpt the action potential waveform and increase firing reliability at a CNS nerve terminal. J Neurosci 30:15479–15490.

Latham A, Paul DH (1971) Spontaneous activity of cerebellar Purkinje cells and their responses to impulses in climbing fibres. J Physiol 213:135–156.

Levin SI, Khaliq ZM, Aman TK, Grieco TM, Kearney JA, Raman IM, Meisler MH (2006) Impaired motor function in mice with cell-specific knockout of sodium channel Scn8a (NaV1.6) in cerebellar Purkinje neurons and granule cells. J Neurophysiol 96:785–793.

Mercer JN, Chan CS, Tkatch T, Held J, Surmeier DJ (2007) Nav1.6 sodium channels are critical to pacemaking and fast spiking in globus pallidus neurons. J Neurosci 27:13552–13566.

Pugh JR, Raman IM (2009) Nothing can be coincidence: synaptic inhibition and plasticity in the cerebellar nuclei. Trends Neurosci 32:170–177.

Raman IM, Bean BP (1997) Resurgent sodium current and action potential formation in dissociated cerebellar Purkinje neurons. J Neurosci 17:4517–4526.

Raman IM, Bean BP (2001) Inactivation and recovery of sodium currents in cerebellar Purkinje neurons: evidence for two mechanisms. Biophys J 80:729–737.

Raman IM, Sprunger LK, Meisler MH, Bean BP (1997) Altered subthreshold sodium currents and disrupted firing patterns in Purkinje neurons of Scn8a mutant mice. Neuron 19:881–891.

Schaller KL, Caldwell JH (2003) Expression and distribution of voltage-gated sodium channels in the cerebellum. Cerebellum 2:2–9.

Thach WT (1968) Discharge of Purkinje and cerebellar nuclear neurons during rapidly alternating arm movements in the monkey. J Neurophysiol 31:785–797.

Theile JW, Jarecki BW, Piekarz AD, Cummins TR (2011) Nav1.7 mutations associated with paroxysmal extreme pain disorder, but not erythromelalgia, enhance Navbeta4 peptide-mediated resurgent sodium currents. J Physiol 589:597–608.

Wang GK, Edrich T, Wang SY (2006) Time-dependent block and resurgent tail currents induced by mouse beta4(154–167) peptide in cardiac Na+ channels. J Gen Physiol 127:277–289.

Yu FH, Westenbroek RE, Silos-Santiago I, McCormick KA, Lawson D, Ge P, Ferriera H, Lilly J, DiStefano PS, Catterall WA, Scheuer T, Curtis R (2003) Sodium channel beta4, a new disulfide-linked auxiliary subunit with similarity to beta2. J Neurosci 23:7577–7585.